Published in "Applied Physics A 84(1-2): 77-85, 2006"
which should be cited to refer to this work.

Structural and optical properties of $Mg_xAl_{1-x}H_y$ gradient thin films: a combinatorial approach

R. Gremaud[1] ⋆, A. Borgschulte[1], C. Chacon[2], J. L. M. van Mechelen[1], H. Schreuders[1], A. Züttel[3], B. Hjörvarsson[2], B. Dam[1], R. Griessen[1]

[1] Department of Physics and Astronomy, Condensed Matter Physics, Vrije Universiteit, De Boelelaan 1081, NL-1081 HV Amsterdam, The Netherlands
[2] Department of Physics, Uppsala University, Box 530, S-751 21, Uppsala, Sweden
[3] Institut de Physique, Université de Fribourg, Ch. du Musée 3, CH-1700 Fribourg, Switzerland

Received: date / Revised version: date

Abstract The structural, optical and dc electrical properties of Mg_xAl_{1-x} ($0.2 \leq x \leq 0.9$) gradient thin films covered with Pd/Mg are investigated before and after exposure to hydrogen. We use Hydrogenography, a novel high-throughput optical technique to map simultaneously all the hydride forming compositions and the kinetics thereof in the gradient thin film. Metallic Mg in the Mg_xAl_{1-x} layer undergoes a metal-to-semiconductor transition and MgH_2 is formed for all Mg fractions x investigated. The presence of an amorphous Mg-Al phase in the thin film phase diagram enhances strongly the kinetics of hydrogenation. In the Al-rich part of the film, a complex H-induced segregation of MgH_2 and Al occurs. This uncommon large-scale segregation is evidenced by metal and hydrogen profiling using Rutherford backscattering spectrometry and resonant nuclear analysis based on the reaction $^1H(^{15}N,\alpha\gamma)^{12}C$. Besides MgH_2, an additional semiconducting phase is found by electrical conductivity measurements around an atomic [Al]/[Mg] ratio of 2 ($x = 0.33$). This suggests that the film is partially transformed into $Mg(AlH_4)_2$ at around this composition.

PACS: 78.20.-e; 68.55.-a; 64.75.+g

Send offprint requests to: R. Gremaud
⋆ *Present address:* Tel.: +31 20 598 79 26, Fax: +31 20 598 79 92
E-mail: gremaudr@nat.vu.nl

1 Introduction

The availability of a safe and effective way to store hydrogen reversibly is one of the major issues for its large scale use as an energy carrier [1].

For this purpose, the ideal hydrogen storage material should have the following properties: high gravimetric and volumetric hydrogen density, fast kinetics of (de)hydrogenation near ambient temperature, long term stability and good thermal conductivity for removing the reaction heat. The availability and affordable price of the alloy constituents is also of importance.

As the understanding of hydride materials developed and their limitations for an application in the automotive sector became clear, attention shifted away from simple binary or ternary hydride systems to compounds or composites consisting of multiple elements. However, the number of possible combinations grows factorially, and with all the parameters to be incorporated, a nearly infinite parameter space opens. In the standard approach followed so far, the exploratory search for new light-weight hydrogen storage materials is very time consuming as a bulk sample is needed for each composition investigated. We present here a new combinatorial method that is capable of exploring typically 10^3 samples simultaneously. It is based on the use of large area thin film samples with controlled chemical composition gradients of two, three or more metal constituents [2,3].

To monitor the hydrogen absorption, we exploit the fact that most complex metal-hydrogen systems undergo a metal-insulator transition upon hydrogen exposure [4–10]. By following the optical changes during hydrogenation [11], we are thus able to map simultaneously all the hydride-forming compositions of the gradient thin film. We use the term *Hydrogenography* for this direct mapping of the hydrides formed in a large compositional gradient sample, enabling the investigation of a full metal-hydrogen ternary phase diagram with one sample.

In the present work, we exemplify this technique with the Mg-Al phase diagram in thin films and the hydrogenation properties thereof. Pure magnesium reacts reversibly with hydrogen to form MgH_2. It is thus considered to be one of the most important candidates for the reversible storage of hydrogen due to its light weight, low cost and high hydrogen gravimetric density (7.6 wt%). However, its hydrogen ab/desorption kinetics is unsatisfactory due to the very low diffusion of hydrogen in MgH_2 [12]. However, preparing nanocrystalline Mg [13] by ball milling and adding transition metals [14,15] or transition metal oxides [16] as catalysts improves the kinetics tremendously. This has initiated many studies on Mg-based hydrides, some of them with Al additions [17–19]. Another promising class of materials for hydrogen storage are the Al-based complex hydrides, since Bogdanovic and Schwickardi showed that the decomposition of sodium alanate, $NaAlH_4$, can be made reversible by the addition of Ti and Fe compounds as catalysts [20]. This stimulated the investigation of many other complex systems [21–24]. Among them, magnesium alanate, $Mg(AlH_4)_2$, with 9.3 wt% of hydrogen, is also a potential hydrogen storage material. It was recently synthesized

in bulk form and its decomposition studied [25,26]. Furthermore, theoretical calculations predict $Mg(AlH_4)_2$ to be a large gap semiconductor [8,9]. The potential synthesis of magnesium alanate from the elements as well as the formation of MgH_2 as a function of the Al content triggered thus our interest for the Mg-Al-H system in gradient thin films.

In this article, we investigate the kinetics, electrical and optical properties and the segregation phenomena of Mg_xAl_{1-x} gradient thin films during hydrogenation. For this we use the Hydrogenography method described above. The method is complemented by ^{15}N Nuclear Resonance Analysis (NRA) and Rutherford Backscattering Spectrometry (RBS). We demonstrate that this approach sheds light on the complex hydrogenation process and thereby helps to optimize multi-component hydrogen storage systems.

2 Experimental

The samples consist of a Mg-Al compositional gradient layer of typically 100 to 200 nm thickness covered with a 1 nm Mg layer to avoid an Al-terminated surface. The layers are capped with 10 nm of Pd to prevent oxidation and promote hydrogen dissociation and absorption. This stack of layers is sputtered at room temperature on 5 x 70 mm glass substrates by off-centered dc/rf magnetron sputtering sources. The argon pressure during deposition is $3\cdot 10^{-3}$ mbar and the background pressure lower than 10^{-8} mbar. The chemical composition range is adjusted by varying the angle of both Mg and Al sources relative to the sample normal. Sputter rates in the center of the sample are determined *in situ* before deposition by a quartz crystal monitor.

The total thickness is measured every 5 mm by a DEKTAK^3 stylus profilometer. The dc electrical resistivity is recorded in a Van der Pauw configuration [27] on electrically separated zones every 3 mm. In the hydrogenated state, the metallic Pd overlayer shunts the semiconducting $Mg_xAl_{1-x}H_y$. To correct for this effect, the $Mg_xAl_{1-x}H_y$ and Pd layer are treated as two parallel resistors [28].

The precise chemical compositions and in-depth homogeneity of the film are determined by Rutherford Backscattering Spectrometry (RBS) using 2 Mev He^+ ions on simultaneously deposited layers on glassy carbon substrates. These substrates do not contribute to the background for energies above approximately 0.5 MeV, allowing a precise determination of the amounts of each element in the sample as a function of depth. Besides the metals (Mg, Al, Pd), the oxygen content is obtained. Moreover, it is also possible to distinguish between oxygen adsorbed at the surface, absorbed in the film or adsorbed at the substrate-film interface. The measured RBS data are analyzed with the RUMP software [29,30]. As Mg and Al have nearly the same atomic number ($z = 12$ and 13, respectively), RBS fits are used to deconvolute the Mg and Al contributions to the spectra. Further details about the RBS method can be found elsewhere, see e.g. [31].

The structural characterization is performed in a Bruker D8 Discover X-ray diffractometer (Cu-Kα, λ=1.5418 Å)

After deposition, metallic films are transferred into an optical cell to monitor their optical transmission during hydrogenation. The whole cell is placed in a furnace to control temperature up to 300 °C. A 150 W diffuse light source illuminates the sample from the substrate side, and a 3-channel (RGB) SONY XC-003 charged-coupled device (CCD) camera monitors the transmitted light. Images during hydrogen ab/desorption processes are taken at different time intervals Δt (1 s $\leq \Delta t \leq$ 100 s) depending on the overall kinetics of the Mg-Al composition under consideration.

Additional reflection and transmission measurements of the hydrogenated state are performed in a Perkin Elmer Lambda 900 diffraction grating spectrometer with an energy range from 0.495 to 6.19 eV (λ = 2500 - 200 nm).

The ^{15}N Nuclear Resonance Analysis (NRA) method is used for hydrogen depth profiling of the sample, and is performed at the Tandem accelerator in Uppsala. The technique is based on the ^{1}H(^{15}N,$\alpha\gamma$)^{12}C nuclear resonance reaction and provides the depth profile as well as the total amount of hydrogen per metallic atom [32]. For the profiling, the sample is bombarded with ^{15}N ions with an energy equal to or above the resonance energy (6.385 MeV). Upon penetration, the ions lose energy, and, at the depth where the ions have reached the resonance energy, the probability for the reaction is greatly enhanced. The depth resolution is typically 1 nm close to the surface but deteriorates with increasing depth due to energy straggling. The 4.43 MeV gamma rays are detected in a BGO detector placed at a distance of 3 cm from the sample at an angle of 0 degree with respect to the incident beam. The diameter of the beam at the surface of the sample is around 1 mm and the ion beam current (N^{2+}) is typically 10-40 nA. The detection limit is of some atomic ppm and the precision is determined by the counting statistics. The accuracy is governed by the quality of the calibration standard and the accuracy of the calculated stopping powers. The values used are from Ziegler [33] and the uncertainty is typically of a few percent. Bragg's rule [34] is used to calculate the stopping cross-sections of the compounds. Tantalum hydride ($TaH_{0.47}$) is used as a calibration sample for the absolute hydrogen concentration determination [35].

3 As-deposited film

The hydrogenation of metal gradient thin films depends strongly on their (micro)structure and local composition. Therefore, an extensive characterization of the lateral gradient as well as of the composition as a function of depth after deposition is of primary importance.

In the as-deposited state, Mg_xAl_{1-x} samples are completely opaque and have shiny metallic surfaces, on the Pd side as well as on the substrate side. The results from RBS measurements are illustrated in fig. 1. For each probed composition x on the gradient sample, the RBS spectrum

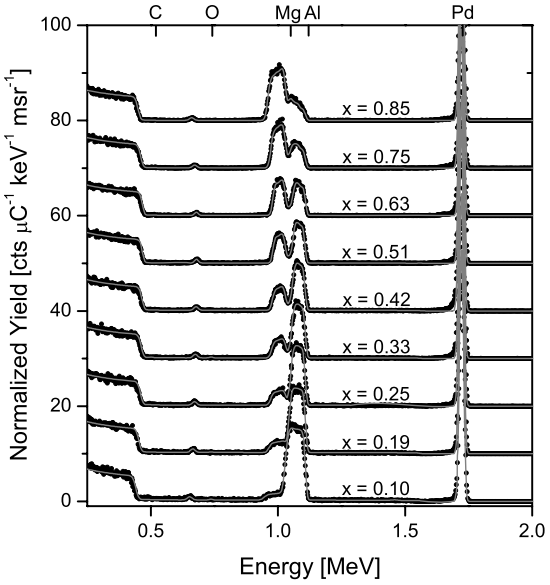

Fig. 1 Solid circles: RBS spectra for various compositions of the as-deposited Pd-capped Mg_xAl_{1-x} gradient thin film on an amorphous C substrate. Top scale: edge (surface) energies for the elements present in the sample. Grey line: fits for (in-depth) homogeneous Mg-Al layers. The obtained Mg fraction x is indicated on the graph.

is compared with the corresponding simulation of an homogeneous Pd/Mg-capped Mg-Al layer. Within the accuracy of the measurement, we conclude that the [Mg]/[Al] ratio is constant over the sample depth for each composition. We do, however, observe some inhomogeneously distributed oxygen. The enthalpies of formation of both magnesium and aluminium oxides ($\Delta H_f(\mathrm{MgO})$ = -601.6 kJ/(mol O), $\Delta H_f(\mathrm{Al_2O_3})$ = -558.6 kJ/(mol O)) are much larger than the ones of the corresponding hydrides ($\Delta H_f(\mathrm{MgH_2})$ = -37.7 kJ/(mol H), $\Delta H_f(\mathrm{AlH_3})$ = -2.8 kJ/(mol H)) [36,37]. Therefore, the chemical purity of the sample is crucial to study the optical and electrical properties upon hydrogenation further. We find oxygen mainly at the substrate-film interface, with an elemental density of $3{\cdot}10^{16}$ at/cm^2 for all measured compositions. As a comparison, this value for as-received amorphous carbon substrates is also $3{\cdot}10^{16}$ at/cm^2. The oxygen amount at the film surface is less than $2{\cdot}10^{15}$ at/cm^2, while the interior of the film appears to be oxygen-free. This shows that the cap-layer provides an effective barrier against oxidation.

Measurements of dc resistivity as a function of hydrogen content or temperature proved to be highly valuable for the study of hydride thin

films [38–40]. At present, our compositional gradient approach also enables us to measure the resistivity as a function of the metallic composition and thus to gain understanding in the related changes of structure for both the as-deposited and the hydrogenated state.

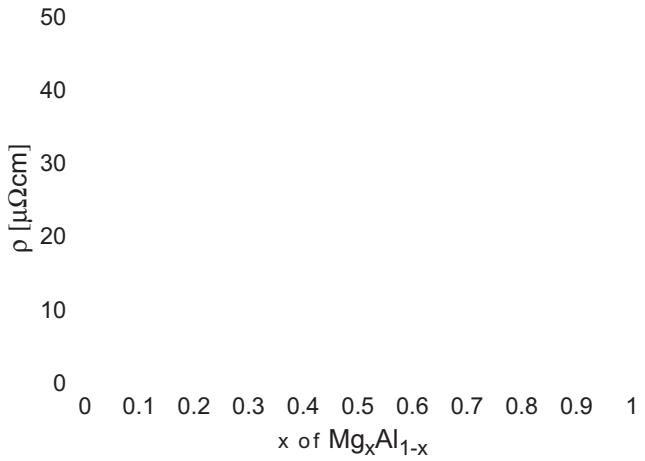

Fig. 2 Filled circles: resistivity ρ of the as-deposited Mg_xAl_{1-x} gradient layer. The fitted parabola centered on $x = 0.49$ reflects the effect of disorder scattering. Results are corrected for the 10 nm Pd cap-layer and normalized to a 200 nm Mg-Al layer thickness. Empty circles: ρ of bulk Mg-Al alloys; taken from ref. [42]

The resistivity ρ of the as-deposited film as a function of composition shows a broad maximum centered at $x = 0.49$ with a maximum $\rho = 47$ $\mu\Omega$cm (Fig. 2). The resistivity then decreases towards the respective pure metal values. On Mg and Al film deposited separately we found $\rho_{\mathrm{Mg}} = 5.69$ $\mu\Omega$cm and $\rho_{\mathrm{Al}} = 3.81$ $\mu\Omega$cm. In the dilute solution limit, ρ exhibits a linear behavior typical for independent scattering processes [41]:

$$\rho(T,x) = \rho_{\mathrm{Al}}(T) + x \cdot \left(\frac{d\rho}{dx}\right)_{\mathrm{Mg}} \qquad 0 \le x \le 0.21 \qquad (1)$$

and

$$\rho(T,x) = \rho_{\mathrm{Mg}}(T) + (1-x) \cdot \left(\frac{d\rho}{dx}\right)_{\mathrm{Al}} \qquad 0.69 \le x \le 1 \qquad (2)$$

We find $\left(\frac{d\rho}{dx}\right)_{\mathrm{Mg}} = 5.8 \pm 0.1$ $\mu\Omega$cm/at% and $\left(\frac{d\rho}{dx}\right)_{\mathrm{Al}} = 9.2 \pm 0.1$ $\mu\Omega$cm/at% for Mg and Al impurities respectively. This linear behavior points to the presence of an extended solid solution of Mg in Al (or Al in Mg) compared to the bulk Mg-Al phase diagram. These extended solubility ranges are indeed supported by X-ray diffraction (XRD), which reveals the

presence of an hcp Mg phase for Mg atomic fractions $x \geq 0.5$ and a fcc Al phase for $x \leq 0.35$ [2].

In its central part, the parabolic shape of the resistivity is characteristic for an electron-impurity dominated conduction and reflects disorder in this Mg-Al mixture. There is no indication of the formation of another alloy phase at an intermediate composition, neither in the resistivity nor in the XRD measurements. In comparison, the bulk resistivity (Fig. 2) clearly shows two dips at approximately $x = 0.5$ and $x = 0.6$. This reduced scattering is attributed to ordered MgAl and $Mg_{17}Al_{12}$ phases formed at these compositions [42]. The absence of these anomalies in the thin film resistivity supports our assumption that the Mg_xAl_{1-x} layer is mainly amorphous in the $0.5 \leq x \leq 0.6$ range.

In summary, the resistivity and XRD measurements of the as-deposited film reveal highly supersaturated single phase solid solutions of Al in Mg ($0.69 \leq x \leq 1$) and Mg in Al ($0 \leq x \leq 0.21$) and an amorphous or microcrystalline glassy metal for $0.5 \leq x \leq 0.6$. For the unspecified regions, we assume a coexistence of the limiting phases. This is consistent with other microstructural studies of Mg-Al coatings deposited by magnetron sputtering [43].

4 Hydrided state

When the as-deposited Mg_xAl_{1-x} metallic gradient thin film is exposed to hydrogen gas, the hydrides which are likely to form are MgH_2 for the Mg-rich part of the gradient and magnesium alanate, $Mg(AlH_4)_2$, at around the composition $x = 0.33$. Indeed, we found indications of the formation of theses two phases [2]. However, the distribution of these hydrides as a function of depth in the film, and hence the segregation occurring between them and the remaining metallic fraction of the film has not been characterized yet. Nuclear Resonance Analysis (NRA) combined with spectral optical transmission measurements give a good understanding of the hydrided part of the active layer. Complementary to this, Rutherford Backscattering Spectrometry (RBS), X-Ray Diffraction (XRD) and conductivity measurements are used to study the metallic fraction after hydrogenation.

4.1 H-induced segregation

The as-sputtered samples consist of Mg and Al homogenously dissolved in Al and Mg, respectively. As already discussed in section 3, the solubility range is larger in thin films than in bulk samples due to the growth process. For most of the compositions, hydrogenation at $T = 110$ °C and $p_{H_2} = 1$ bar forces the system to segregate into the thermodynamically most stable phases MgH_2 and Al [18,19].

This process is investigated by X-ray diffraction. Figure 3 shows X-ray patterns of a $Mg_{0.2}Al_{0.8}$ film during hydrogenation. The initial spectrum

Layer	**Elemental density** $[10^{15}\text{at} \cdot \text{cm}^{-2}]$				$\mathbf{Mg}_x\mathbf{Al}_{1-x}$	**[H]/[M]**
	Pd	Mg	Al	H	x	y
1	68	-	-	-	-	-
2	1	28	275	41	0.09	0.14
3	1	36	250	54	0.13	0.19
4	-	22	110	30	0.17	0.23
5	-	61	36	73	0.63	0.75

Table 1 $Mg_{0.2}Al_{0.8}$ after hydrogenation: result of the RUMP modeling of the RBS measurement. Layer 1 represents the Pd cap-layer and 5 the layer closest to the substrate.

is attributed to a single Al 111 reflection originating from a homogenous Al-phase with a slightly increased lattice parameter due to dissolved Mg. During *in situ* hydrogenation a second peak evolves, which quickly grows, while the original one disappears (see Fig. 3)). The corresponding lattice parameter of the evolving peak is that of pure aluminium. Thus, we have followed the decomposition of Al(Mg) into pure Al and probably MgH_2. X-ray peaks of MgH_2 have not been detected, presumably due to too small a grain size of the precipitates.

To measure the hydrogen content directly, the hydrogenated Mg_xAl_{1-x} gradient film is probed by NRA. In fig. 4, the data have been compiled into a hydrogen depth profile as a function of the Mg-Al content. It demonstrates that the hydrogen distribution in the film depends markedly on the alloy composition x.

However, without the information of the metal distribution inside the film, a distinct proof for the formation of a particular hydride is difficult. RBS can deliver the elemental depth profile of a thin film. For this, we fitted the RBS spectrum of the hydrogenated film, keeping the total number of Mg and Al atoms as determined in the as-deposited state constant. Furthermore, we implement the hydrogen content determined by NRA in the fit to account for the reduction of the (planar) density after hydrogenation. The RBS spectra of a Mg-rich and an Al-rich Mg-Al film after hydrogenation are shown in fig. 5. Mg-rich films with $x \geq 0.5$ show a uniform distribution of Mg and Al, while it is clearly evident that Al-rich films ($x \leq 0.2$) are enriched in Mg at the interface.

With these two pieces of information we can draw a detailed description of the segregation phenomenon in Mg-Al films during hydrogenation. Mg-rich films ($x \geq 0.5$) show a uniform distribution of hydrogen and metal atoms. Here, the hydrogen depletion at the surface is due to a partial unloading of the film during measurement. At these low Al-concentrations, Al is dissolved in the Mg-matrix. During magnesium hydride formation small Al-clusters are formed (see section 4.2), which are uniformly dispersed in

the MgH_2-matrix. The small Al clusters impede the formation of a MgH_2-blocking layer [44], and indeed, the kinetics of Al-doped Mg-films is enhanced compared to pure magnesium. This qualitative explanation is in agreement with the optical and kinetics measurements reported in the next section.

At higher Al-concentrations ($x < 0.5$), the transport of metal atoms becomes rate-limiting, and the rate constant of the kinetics is of the order of the diffusion constant of Al in Mg [45]. This explains the slower kinetics at these Al-contents, since for the nucleation and growth of the hydride more Al has to be (re)moved. Furthermore, as in similar fcc metals, hydrogen diffusion is very slow in Al [46]. This implies that the observed percolation (see section 4.4) of the top metallic layers hinders further hydrogenation. This would explain the hydrogen enrichment at the surface of Mg-Al films for $0.4 < x < 0.5$ (Fig. 4).

However, this explanation does not hold anymore for Al-rich Mg_xAl_{1-x} films ($x < 0.25$). Here, a strong hydrogen enrichment at the interface is evident. RBS combined with NRA results clearly indicate a segregation of Al and MgH_2 followed by a migration of Al towards the surface and of MgH_2 towards the interface. Why these phases migrate to different interfaces is not clear yet.

It is worthwhile to note that the reported segregation is purely H-induced. Annealing the as-deposited samples in vacuum at 110 °C does not produce such compositional inhomogeneities.

Finally, no segregation, and a slightly higher hydrogen content is found around the [Mg]/[Al] = 2 ratio (Fig. 4b). This is also corroborated by optical and electrical measurements (Fig. 6 and 9). Interestingly, it is the right ratio to form $Mg(AlH_4))_2$, and probably a small amount of it is present in the film (see section 6).

4.2 Hydrogenography

By applying 1.1 bar hydrogen pressure at 110°C, some regions of the sample become transmissive (Fig. 6). After 10^3 s of hydrogen exposure, Mg_xAl_{1-x} with $0.5 < x < 0.69$ displays a color neutral transmission (Fig. 6a). It is important to note that the segregation processes reported in section 4.1 have hardly started yet at this time (see Fig. 3). We assume therefore that the film is still homogeneous over its entire thickness. The intensity, which is highest at $x = 0.69$, decreases linearly with decreasing Mg content, and has a cutoff at $x = 0.5$ (Fig. 6c). We attribute this behavior to the formation of MgH_2, which is a colorless insulator with a band gap of 5.6 eV [47]. From NRA measurements, the in-depth integrated [H]/[Mg] ratio at these compositions is between 1.7 and 1.5. This means that 75% to 85% of the Mg is transformed into MgH_2. This is in good agreement with Johansson et al., who found similar unreacted Mg fractions in thin hydrogenated Mg-Ni wedged films [48].

From the low transmission in fig. 6, we notice that our film is still incompletely hydrogenated for $0.69 \leq x \leq 1$. In this composition range, it exhibits a hydrogenation behavior similar to that in pure Mg films, whose hydrogen uptake is kinetically hindered by a dense surface layer of MgH_2 [49]. This is not astonishing if we consider that in the as-deposited state, our film consists of an extended solid solution of Al in Mg in this range.

For $0.5 < x < 0.69$, hydrogenation occurs already within 10^3 s. There are two factors explaining a faster kinetics at these Al-richer compositions: Firstly, Mg crystallinity is decreased due to the presence of the Mg-Al amorphous phase [50]. Secondly, the presence of Al at the surface of Mg grains will speed up the hydrogen uptake, as it is the case for surface Ni [5,44,51] or MgO_x [52].

Finally, Al-rich compositions ($x < 0.5$) have not absorbed enough hydrogen at $t = 10^3$ s to exhibit a significant transmission.

After 10^5 s of hydrogen exposure, Mg fractions above $x = 0.69$ have hydrided. Furthermore, an additional feature has appeared in transmission in the Al-rich region (Fig. 6b): a broad peak is present for $0.26 \leq x \leq 0.36$. This transmission is centered around an [Al]/[Mg] ratio of 2 ($x = 0.33$), suggesting the formation of $Mg(AlH_4)_2$.

4.3 Optical spectra

To clarify the nature of the optical features present in the Al-rich part of the sample after 10^5 s of hydrogen exposure, we measure the transmission of hydrogenated films from 0.5 to 6 eV. To maximize the transmission, the Mg-Al layer is only 40 nm thick, capped with 8 nm of Pd. The samples are deposited on quartz substrates. The measured spectra are compared with calculations based on two extreme cases :

1. Homogeneous mixture:
   For a given composition x, the $Mg_xAl_{1-x}H_y$ sample is an homogeneous mixture of MgH_2 and Al. Its dielectric function $\langle\tilde{\epsilon}\rangle$ is described by an effective medium theory if the grain size of the respective particles is smaller than the wavelength of light. We use Bruggeman's approximation for spherical particles. $\langle\tilde{\epsilon}\rangle$ is then implicitly given by [53]:

   $$f_A \frac{\tilde{\epsilon}_A - \langle\tilde{\epsilon}\rangle}{\tilde{\epsilon}_A + 2\langle\tilde{\epsilon}\rangle} + f_B \frac{\tilde{\epsilon}_B - \langle\tilde{\epsilon}\rangle}{\tilde{\epsilon}_B + 2\langle\tilde{\epsilon}\rangle} = 0 \quad (3)$$

   $f_{A,B}$ and $\tilde{\epsilon}_{A,B}$ are the volume fractions and the complex dielectric functions of the phase A (MgH_2) and B (Al), respectively. The transmission of the Pd-capped Mg-Al layer is then calculated.

2. Layered segregation:
   The H-induced segregation is fully reached and the sample consists of a $Pd/MgH_2/Al$ stack.

Figure 7 displays the measured and calculated transmission for the compositions $x = 0.32$, 0.39 and 0.51. For $x = 0.51$ and 0.32, the measured spectrum fits reasonably well with the one calculated for an homogeneous Mg-Al layer. Moreover, calculations of a segregated layer predict a broad peak around 4.5, or, respectively 5.5 eV, which is not observed experimentally. At an intermediate composition ($x = 0.39$), we do observe an additional peak at high energies (4.5 eV) which can be related to segregation. Note that the calculations for an homogeneous MgH_2-Al mixture yield always a larger transmission than the segregated ones in the visible range (from 1.2 to 3 eV), which we use for hydrogen mapping with our CCD. Partly segregated MgH_2 could then account for the low intensity observed in the $0.39 \leq x \leq 0.5$ range (see Fig. 6), while the higher intensity observed around $x = 0.33$ is well fitted by an homogeneous mixture of MgH_2 and Al. For higher Al contents ($x \leq 0.2$), RBS and NRA measurements (see section 4.1) show that MgH_2 segregates strongly towards the quartz substrate. However, the intensity is too low ($< 1\%$) for an optical analysis.

As complex segregation phenomena occur while hydrogenating the Mg-Al gradient, it is difficult to model the exact shape of a transmission spectrum at a given composition. However, the (non)-occurrence and respective position in energy of the different transmission peaks are characteristic for each composition. Moreover, for 40 nm films, the interference maxima due to the layer thickness are approximately 15 eV apart and do not contribute significantly to the shape of the transmission spectrum. Therefore, each spectrum becomes a "fingerprint" of the corresponding composition and gives a qualitative understanding of the process contributing most to the optics. To illustrate this, the transmission spectra in the range $0.36 \leq x \leq 0.58$ are displayed in Figure 8. They can be schematically assigned to three groups: from $x = 0.58$ to 0.51, the film is homogeneous over its thickness, the peak around 6 eV for $x = 0.51$ and 0.54 being the signature for the unreacted Mg fraction mixed with MgH_2 and Al. From $x = 0.47$ to 0.38, the peak around 4.5 eV accounts for the MgH_2/Al segregation in the sample. Finally the sample becomes homogeneous again for a composition $x = 0.36$.

4.4 Conductivity

For a characterization of the metallic fraction present in the gradient thin film, we study the dc conductivity σ as a function of composition. Figure 9 displays σ before and after hydrogenation for $3{\cdot}10^5$ s at $p = 1.1$ bar H_2 and $T = 110$ °C. As previously mentioned, conductivity variations in the as-deposited state are small because of the metallic nature of the film. In the hydrogenated state, it changes drastically: The Mg-rich part becomes semiconducting, with a conductivity below 1 (m Ω cm)$^{-1}$. A striking feature is the positive conductivity shift in the Al-rich part ($0.15 < x < 0.5$) after hydrogenation. An increase of the Al grain size would account for this effect by shortening the current paths and reducing the intergrain contact

resistances. From XRD measurements we indeed find an increase of the Al 111 reflection and a shift of the lattice parameter toward the bulk value during hydrogenation (See Fig. 3).

For all Mg compositions $x \leq 0.61$, the overall behavior of σ is well described by a power law:

$$\sigma \propto (v - v_c)^{\beta} \propto (x_c - x)^{\beta} \tag{4}$$

with a critical volume fraction of Al metal $v_c = 0.25 \pm 0.01$ corresponding to an atomic Mg fraction $x_c = 0.61 \pm 0.01$ and a critical exponent $\beta = 1.5 \pm 0.1$. These values are in agreement with a simple cubic bond percolation model that predicts $v_c = 0.25$ and $\beta = 1.6 \pm 0.1$ [54,55]. This is consistent with the conclusion that the sample consists of MgH_2 inclusions in Al.

However, the lower conductivity observed for $0.26 \leq x \leq 0.36$ is not reproduced by the model of Al percolation in MgH_2. The compositional range of the conductivity deviation corresponds well to that of the optical transmission feature observed in section 4.2. This indicates that less Al contributes to the conduction and may be involved in the formation of a small amount of insulating $Mg(AlH_4)_2$ phase. However, no deviation from the model is found for $0.4 < x < 0.5$. This suggests that the slightly higher, inhomogeneous transmission observed in this range (see Fig. 6) does not involve any Mg-Al-H compound and is due to MgH_2 which is formed from the purely amorphous Mg-Al phase [43]. Theoretical calculations predict $Mg(AlH_4)_2$ to be a large band gap semiconductor [8,9]. However, the deviation in conductivity measured for $0.25 < x < 0.35$ is small compared to the contribution of the MgH_2-Al mixture. From measurements of the film expansion after hydrogenation, we estimate that less than 5% of the film is transformed into $Mg(AlH_4)_2$.

5 Kinetics

Hydrogenography makes it also possible to follow in detail the kinetics of hydrogen uptake of Mg_xAl_{1-x}. Figure 10 (b) gives the temporal evolution of the transmission upon hydrogenation for $0.2 \leq x \leq 0.71$. Hydrogenation starts first at around a nominal composition of Mg_2Al after 10^2 s (Fig. 10c). The transmission extends gradually towards the MgAl nominal composition before 10^3 s. By comparison with Fig. 6c, we conclude that this transmission lobe is induced by MgH_2, with a loading time $\tau = 200$ s for the fastest composition at around $x = 0.67$ (Fig. 10c). Here τ is defined as the time where $\log T = 1/2 \log(T_{max})$, taking the final transmission level T_{max} as fully loaded. For Mg fractions higher than $x = 0.68$, the formation of a MgH_2 blocking layer reduces the hydrogenation kinetics substantially and increases τ to $1.5 \cdot 10^3$ s for $x = 0.7$. As this change in uptake rate is occurring at the limit of the Al solubility in Mg, we conclude that an admixture of the amorphous Mg-Al phase to the Mg(Al) phase improves the hydrogenation kinetics dramatically.

As discussed in section 4.1 previously, compositions between $x = 0.5$ and 0.38 still exhibit a low transmission after 10^3 s because of the H-induced segregation of Mg_xAl_{1-x} into MgH_2 and Al. For Al-richer compositions, a second transmission lobe develops at around a nominal composition of $MgAl_2$ ($x \simeq 0.33$) (Fig. 10b) with a loading time of 10^4 s.

We attribute this rise in transmission to an homogeneous mixture of MgH_2, Al and possibly $Mg(AlH_4)_2$ (at most 5%). Its slower kinetics is related to the slow diffusion of the metal atoms.

Finally, for composition of $x \leq 0.2$, no significant rise in transmission occurs. Although MgH_2 present in the sample segregates towards the substrate (see section 4.1), the thick Al layer on top prevents transmission.

6 Conclusions

Hydrogenography, i.e. the thin film analysis techniques combined with the use of compositional gradient samples, enables us a detailed understanding of the hydrogenation of Mg_xAl_{1-x} alloys:

The first important result is that hydrogenation of Mg_xAl_{1-x} thin films occurs at much milder conditions ($p(H_2) = 1.1$ bar and $T = 110°C$) than in the corresponding bulk samples. Another advantage is that the mapping by optical transmission of the hydrides and the kinetics of the formation thereof is possible throughout the entire film simultaneously. Under these conditions, MgH_2 is found to form at all alloy compositions investigated ($0.2 \leq x \leq 0.9$). An extrapolation of the integrated hydrogen content towards Al-richer compositions (see Fig. 4b) shows that MgH_2 would form even in Mg-Al alloys containing a Mg fraction as low as 5%.

However, a comprehensive characterization of the as-deposited film, as well as the knowledge of the structural changes occurring during hydrogenation are essential for the analysis of the optical measurements. Resistivity and XRD measurements as a function of the Mg fraction x in the as-deposited metallic state show that Mg-Al alloys in thin film form do not follow the bulk phase diagram. The extended metallic solubility ranges and the absence of ordered phases in the as-deposited state determine the overall behavior of the kinetics. The ability to probe an almost continuous set of compositions shows that the best kinetics of hydrogen absorption is achieved for the Mg-richer composition ($x = 0.68$) containing the amorphous (or nanocrystalline) Mg-Al alloy. This also points out the importance of thin sputtered films as an alternative to ball-milling to obtain glassy metastable phases and therefore to optimize the hydrogenation kinetics.

Although the morphology of the as-deposited film clarifies the kinetics of the Mg-rich part of the sample, it does not explain the complex pattern behavior of the optical transmission observed for Al-rich compositions in the hydrogenated state. Joined NRA, RBS and optical spectra measurements provide complementary information on the large-scale hydrogen-induced segregation that occurrs at these compositions. The occurrence and direction of the MgH_2 migration is found to depend strongly on the Mg fraction

x. For Mg dissolved in the Al lattice ($x \leq 0.21$), RBS and NRA measurements show clearly that MgH_2 strongly segregates towards the substrate. It is as yet unclear which process triggers the direction of the MgH_2 (and Al) migration.

Unreacted Mg, as well as the degree of (in)homogeneity of the whole Mg_xAl_{1-x} layer are also detected by an optical transmission-energy spectrum, even for Mg fractions ($0.36 < x < 0.5$) for which the segregation is happening on a smaller scale, and thus is difficult to resolve by NRA. This shows the complementarity of optical transmission, that probes directly the full stack of layers, with depth sensitive ion beam techniques like NRA and RBS. The comparison between measured optical spectra and the simulated ones also explains the low transmission intensity observed during kinetics experiments for this compositional range. In this case, the starting alloy is an amorphous Mg-Al alloy, and the MgH_2 forms preferentially towards the Pd surface.

The two above examples show the variety of possible segregation phenomena in a single metal-hydride system and the potential of thin film related techniques to study these in relation to the hydrogenation process.

For Mg fractions $0.25 \leq x \leq 0.36$, the film is found to be homogeneous in depth for both NRA and optical measurements. The observed optical transmission would account for a mixture of MgH_2 and Al. However, the [Al]/[Mg] ratio of 2, together with the following experimental facts indicate that a fraction of the whole layer has transformed into $Mg(AlH_4)_2$:

1. The integrated hydrogen content is slightly higher than the normal linear increase as a function of Mg fraction.
2. An anomalous conductivity behavior points to the presence of an additional semiconducting phase in the layer around $x = 0.33$.

This investigation of the Mg-Al-H system demonstrates the great potential of our compositional thin film approach for the search for new light-weight metal hydride storage materials. The ability to investigate hundreds of alloy compositions in a single thin film, the characterization of their microstructure before and after hydrogen loading and the determination of the most favorable kinetics enables us to optimize efficiently complex metal-hydride systems whose hydrogenation depends on a subtle interplay of thermodynamic stability, atomic diffusion of all constituents and surface catalysis.

Acknowledgements Financial support by the Dutch Foundation for Fundamental Research on Matter (Stichting voor Fundamenteel Onderzoek der Materie, FOM) through the ACTS "Sustainable Hydrogen" program and the Swiss Federal Office for Energy (Bundesamt für Energie, BfE) is gratefully acknowledged.

References

1. L. Schlapbach, A. Züttel: Nature **414**, 353 (2001)

2. R. Gremaud, A. Borgschulte, W. Lohstroh, H. Schreuders, A. Züttel, B. Dam, R. Griessen: J. Alloys Compd. **404-406**, 775 (2005)
3. M. Pasturel, M. Slaman, H. Schreuders, J. H. Rector, D. M. Borsa, B. Dam, R. Griessen: submitted to J. App. Phys.
4. A. Peles, J. A. Alford, Zhu Ma, Li Yang, M. Y. Chou: Phys. Rev. B **70**, 165105 (2004)
5. T. J. Richardson, J. L. Slack, R. D. Armitage, R. Kostecki, B. Farangis, M. D. Rubin: Appl. Phys. Lett. **78**, 1 (2001)
6. J. L. M. van Mechelen, B. Noheda, W. Lohstroh, R. J. Westerwaal, J. H. Rector, B. Dam, R. Griessen: Appl. Phys. Lett. **84**, 3653 (2004)
7. W. Lohstroh, R. J. Westerwaal, B. Noheda, S. Enache, I. A. M. E. Giebels, B. Dam, R. Griessen: Phys. Rev. Lett. **93**, 197404 (2004)
8. M. J. van Setten, G. A. de Wijs, V. A. Popa, G. Brocks: Phys. Rev. B **72**, 073107 (2005)
9. O. M. Løvvik, P. N. Nolin: Phys. Rev. B **72**, 073201 (2005)
10. O. M. Løvvik: Phys. Rev. B **71**, 144111 (2005)
11. A. Borgschulte, R. J. Westerwaal, J. H. Rector, B. Dam, R. Griessen: App. Phys. Lett. **85**, 4884 (2004)
12. A. Krozer, B. Kasemo: J. Less-Common Met. **160**, 323 (1990)
13. A. Zaluska, L. Zaluski, J. O. Ström-Olsen: J. Alloys Compd. **288**, 217 (1999)
14. G. Liang, J. Huot, S. Boily, A. van Neste, R. Schulz: J. Alloys Compd. **292**, 247 (1999)
15. J. F. Pelletier, J. Huot, M. Sutton, R. Schulz, A. R. Sandy, L. B. Lurio, S. G. J. Mochrie: Phys. Rev. B **63**, 052103 (2001)
16. W. Oelerich, T. Klassen, R. Bormann: J. Alloys Compd. **315**, 237, (2001)
17. Y. Song, X. Guo, R. Yang: Phys. Rev. B **69**, 094205 (2004)
18. A. Zaluska, L. Zaluski, J. O. Ström-Olsen: Appl. Phys. A **72**, 157 (2001)
19. S. Bouaricha, J. P. Dodelet, D. Guay, J. Huot, S. Boily, R. Schulz: J. Alloys Compd. **297**, 282 (2000)
20. B. Bogdanovic, R. A. Brand, A. Marjanovic, M. Schwickardi: J. Alloys Compd. **302**, 36 (2000)
21. A. Züttel, P. Wenger, S. Rentsch, P. Sudan, Ph. Mauron, Ch. Emmenneger: J. Power Sources **118** 1 (2003)
22. B. C. Hauback, H. W. Brinks, H. Fjellvåg: J. Alloys Compd. **346** 184 (2002)
23. H. W. Brinks, B. C. Hauback: J. Alloys Compd. **354** 143 (2003)
24. H. Morioka, K. Kakizaki, S. Chung, A. Yamada: J. Alloys Compd. **353** 310 (2003)
25. M. Fichtner, O. Fuhr: J. Alloys Compd. **345**, 286 (2002)
26. M. Fichtner, J. Engel, O. Fuhr, A. Gloess, O. Rubner, R. Ahlrich: Inorg. Chem. **42**, 7060 (2003)
27. L. J. Van der Pauw: Philips Res. Rep. **13**, 1 (1958)
28. A. T. M. van Gogh, D. G. Nagengast, E. S. Kooij, N. J. Koeman, J. H. Rector, R. Griessen: Phys. Rev. B **63**, 195105 (2001)
29. L. R. Doolittle: Nucl. Instr. Meth. Phys. Res. **B15**, 227 (1985)
30. http://www.genplot.com
31. L. C. Feldman, J. W. Mayer: *Fundamentals of surface and thin film analysis*, (Elsevier, New York 1986)
32. W. Lanford, H. Trautvetter, J. Ziegler, J. Keller: Appl. Phys. Lett. 28, 566 (1976)

33. J. F. Ziegler: *The stopping and ranges of ions in matter*, in *Handbook of Stopping Cross-Sections for Energetics Ions in all Elements*, Vol. **5**, (Pergamon Press, New York 1980)
34. W. K. Chu, J. W. Mayer, M. A. Nicolet: *Backscattering Spectrometry*, (Academic Press, New York 1978)
35. B. Hjörvarsson, H. Rydén, T. Ericsson, E. Karlsson: Nucl. Instr. Meth. Phys. Res. **B42**, 257 (1989)
36. D. R. Lide: *CRC handbook of chemistry and physics*, (CRC press, 2005)
37. P. Claudy , B. Bonnetot, J. M. Letoffe: Thermochim. Acta **27**, 205 (1978)
38. J. N. Huiberts, R. Griessen, J. H. Rector, R. J. Wijngaarden, J. P. Dekker, D. G. de Groot, N. J. Koeman: Nature **380** (1996) 231
39. I. A. M. E. Giebels, J. Isidorsson, R. Griessen: Phys. Rev. B **69**, 205111 (2004)
40. S. Enache, W. Lohstroh, R. Griessen: Phys. Rev. B **69**, 115326 (2004)
41. N. F. Mott, H. Jones: *The theory of the properties of metals and alloys*, (Dover Pub, London 1936)
42. R. W. Klaffky, N. S. Mohan, D. H. Damon: J. Phys. Chem. Solids, 36 (10), 1147 (1975)
43. R. D. Arnell, R. I. Bates: Vacuum **43**, 105 (1992)
44. G. Friedlmeier, M. Groll: J. Alloys Compd. **253**, 550 (1997)
45. C. J. Smithells: *Smithells Metals Reference Book (7th Ed.)*, (Butterworth-Heinemann, Oxford 1992)
46. Y. Adda, J. Philibert: *La diffusion dans les solides* (Presses universitaires de France, Paris 1966)
47. J. Isidorsson, I. A. M. E. Giebels, H. Arwin, R. Griessen: Phys. Rev. B **68**, 115112 (2003)
48. E. Johansson: *Synthesis and characterization of potential hydrogen storage materials*, (Acta Universitatis Upsaliensis, Uppsala 2004)
49. J. Rydén, B. Hörvarsson, T. Ericsson, E. Karlsson, A. Krozer, B. Kasemo: J. Less-Common Met. **152**, 295 (1989)
50. K. Higuchi, H. Kajioka , K. Toiyama , H. Fujii , S. Orimo, Y. Kikuchi: J. Alloys Compd. **293-295**, 484 (1996)
51. F. G. Heisenberg, D. A. Zagnoli, J. J. Sheridan: J.Less-Common Met. **74**, 323 (1980)
52. P. Hjort, A. Krozer, B. Kasemo: J. Alloys Compd. **237**, 74 (1996)
53. G. A. Niklasson, C. G. Granqvist: J. App. Phys **55**, 3382, (1984)
54. D. Stauffer, A. Aharony: *Introduction to percolation theory*, (Taylor and Francis, London 1994)
55. S. Kirkpatrick: Rev. Mod. Phys. **45**, 574 (1973)

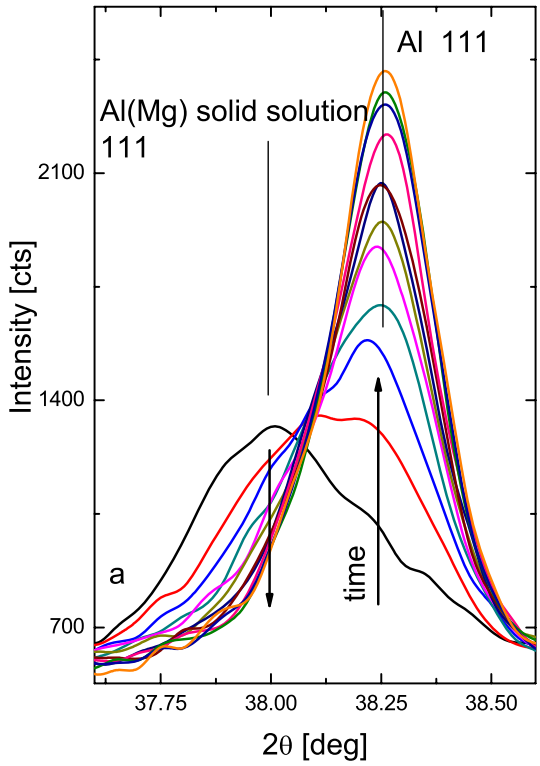

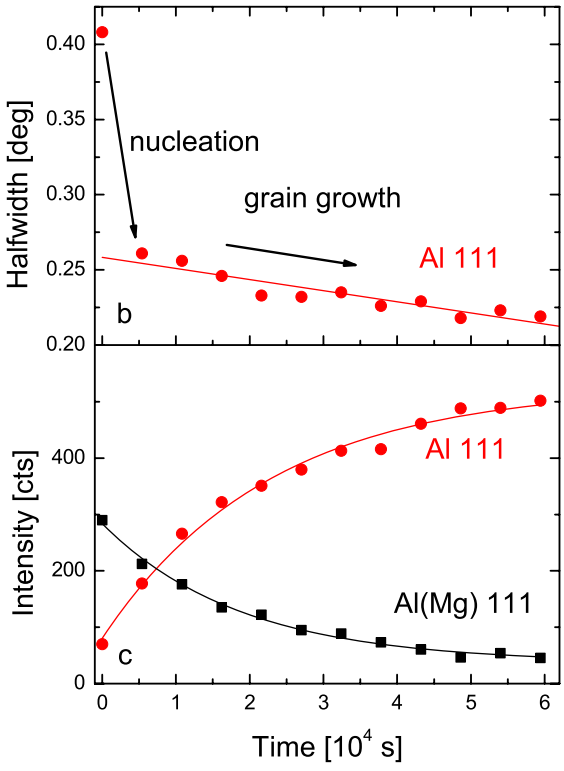

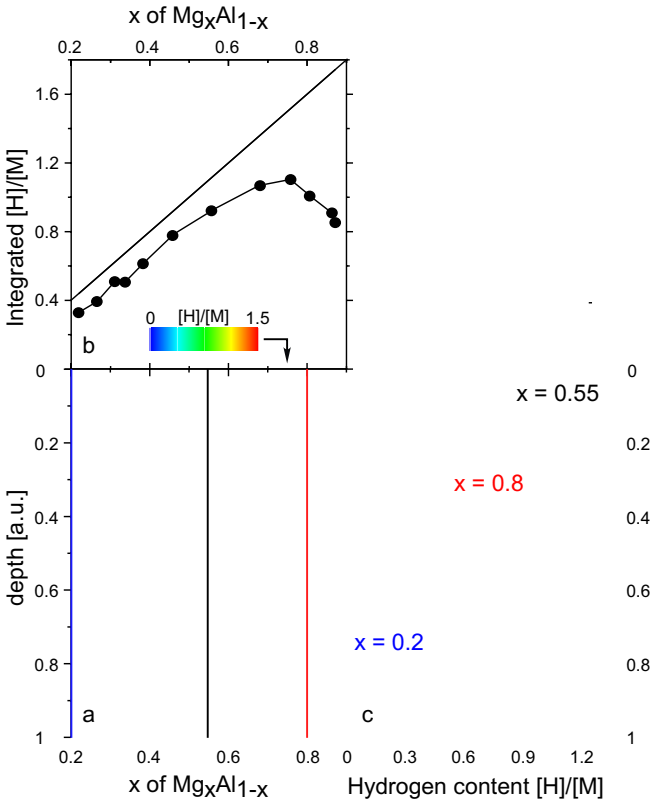

Fig. 4 Nuclear Resonance Analysis (NRA) is used for hydrogen depth profiling of hydrided Pd-capped Mg_xAl_{1-x} films. (**a**) Contour plot of the hydrogen-to-metal ratio [H]/[M] as a function of film depth and magnesium fraction x of the Mg_xAl_{1-x} layer. The thickness of the film is normalized for all compositions. A depth of 0 corresponds to the (Pd-) surface, while 1 indicates the substrate interface. (**b**) Filled circles, [H]/[M] integrated over the film thickness, as a function of the Mg fraction x. The decrease of hydrogen content for Mg-rich compositions is due to unloading of the surface during the transfer of the sample in air. The full line indicates the theoretical maximum [H]/[M] for a mixture of MgH_2 and Al. (**c**) [H]/[M] depth profile for a mainly uniform hydrogen distribution (red, x = 0.8), a hydrogen enrichment at the surface (black, x = 0.55), and a hydrogen enrichment at the interface with the substrate (blue, x = 0.2), respectively.

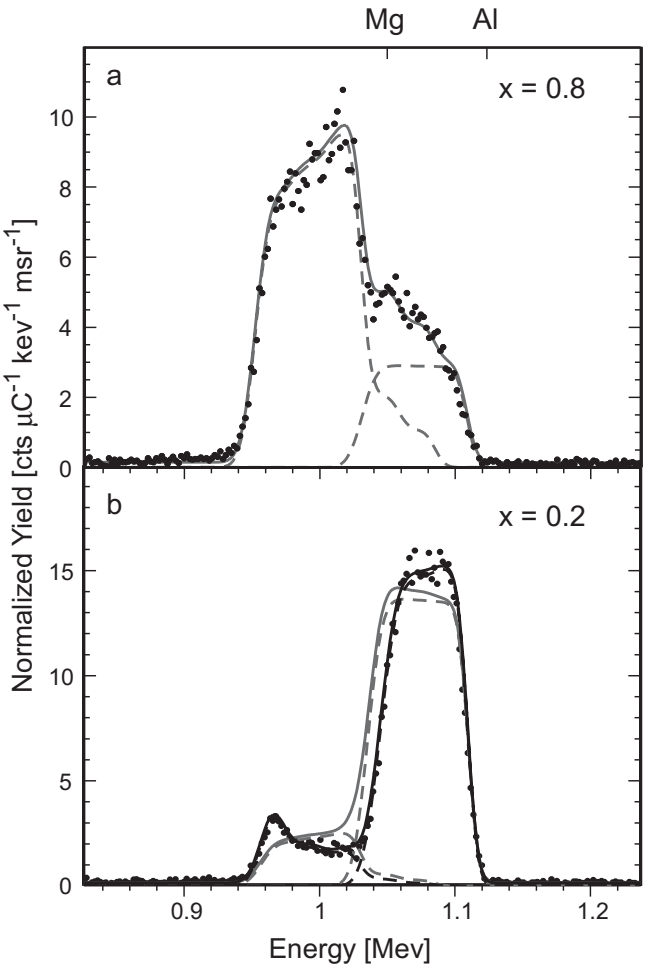

Fig. 5 The Mg and Al contributions to RBS spectra of hydrogenated $Mg_xAl_{1-x}H_y$ layers. (**a**) $x = 0.8$, hydrogen-to-metal ratio $y = [H]/[M] = 0.5$. Full line, fit for an homogeneous layer. (**b**) $x = 0.2$, $y = 0.3$. Full line (gray), fit for an homogeneous layer, (black) fit for a segregation of Al towards the film surface and MgH_2 towards the interface (see Table 1). Dashed lines show the separate Mg and Al contribution. Top scale: Edge (surface) energies for Mg and Al.

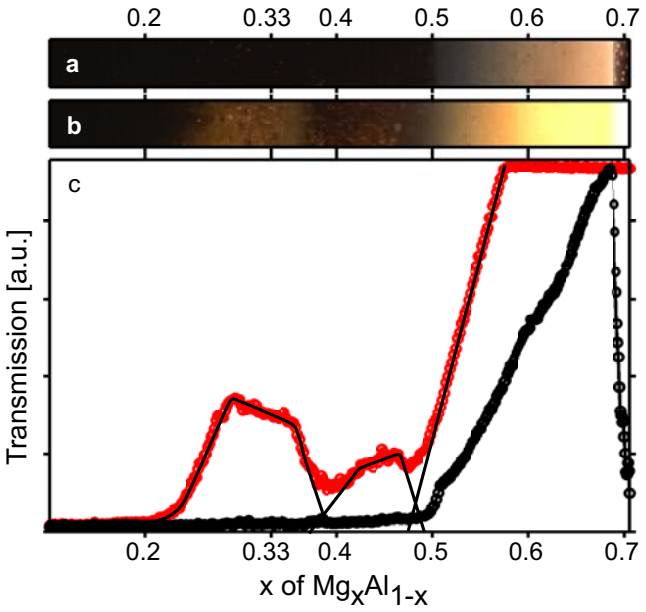

Fig. 6 Mg-Al gradient sample hydrogenated at $T = 110°C$ and $p(H_2) = 1.1$ bar. Transmission image after (**a**) 10^3 s, (**b**) 10^5 s hydrogen exposure time. (**c**) CCD red channel transmission as a function of composition. Black circles: after 10^3 s, red circles: after 10^5 s. Black lines indicate schematically the contributions of the various phases discussed in the text.

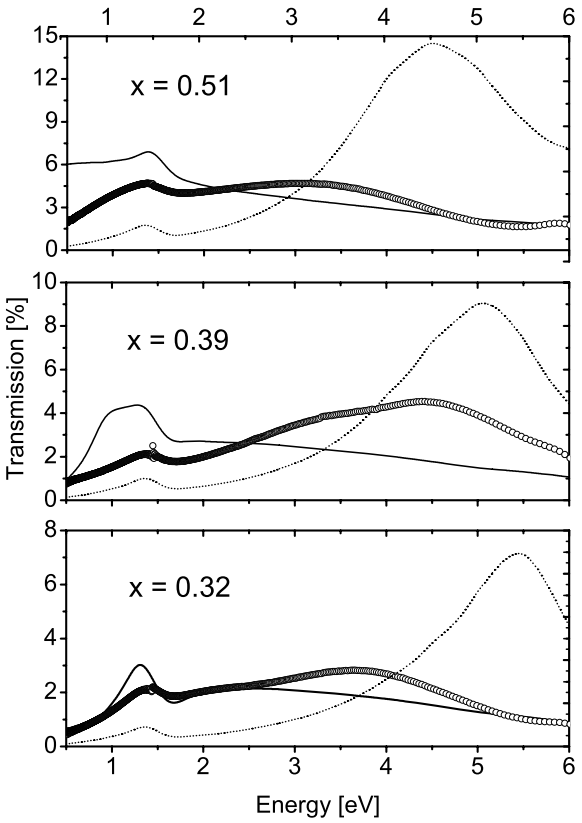

Fig. 7 Comparison between experimental and theoretical optical transmission spectra for a 40 nm $Mg_xAl_{1-x}H_y$ film capped with 8 nm of Pd. (o) Measured spectra for $x = 0.32$, 0.39 and 0.51. Solid lines, calculations based on homogeneous mixtures of MgH_2 and Al by the Bruggeman approximation. Dashed line, calculations for fully segregated MgH_2 and Al bilayers.

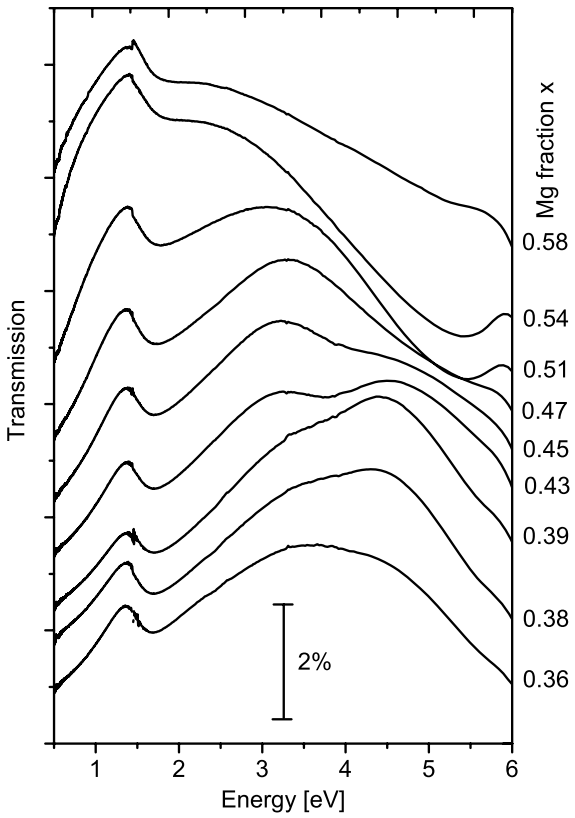

Fig. 8 Optical transmission of a 40 nm $Mg_xAl_{1-x}H_y$ film capped with 8 nm Pd as a function of light energy. A shift of 0.8% in transmission intensity is added between two consecutive spectra for clarity.

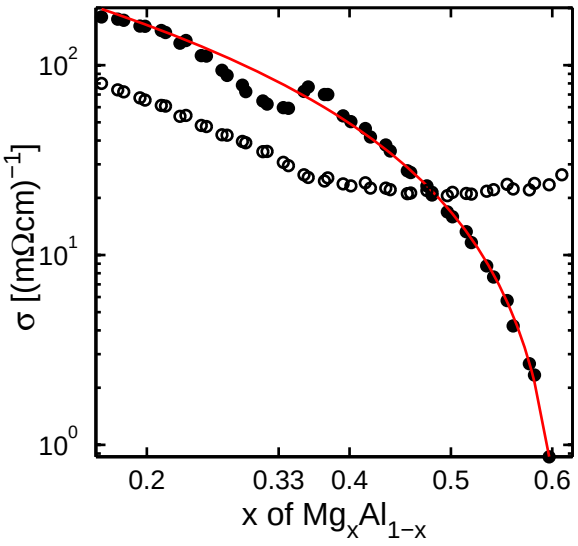

Fig. 9 Conductivity σ of the Mg_xAl_{1-x} layer in the as-deposited state (empty circle) and in the hydrogenated state (filled circles). Data are corrected for the 10 nm Pd cap-layer and normalized to a 200 nm Mg-Al layer thickness. The solid line is a fit of the data based on a simple cubic bond percolation model (critical Al volume fraction $v_c = 0.254$, critical exponent $\beta = 1.5$).

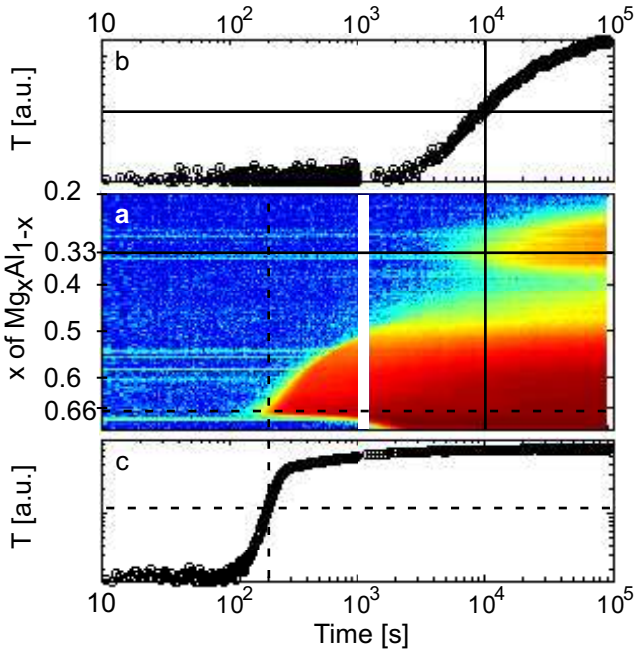

Fig. 10 Evolution of the optical transmission (from the CCD, bandwidth from 1.1 to 3.3 eV) of a Mg_xAl_{1-x} gradient layer capped with 10 Pd during hydrogenation at 110 °C and $p(H_2) = 1.1$ bar. The composition x varies from $x = 0.2$ to $x = 0.71$. (**a**) Contour plot of the transmission as a function of Mg fraction x and time. Blue corresponds to low transmission and red to high transmission. (**b**) Transmission for $x = 0.32 \pm 0.01$ (**c**) Transmission for the fastest hydriding composition of MgH_2 + Al in Mg_xAl_{1-x} with $x = 0.67 \pm 0.01$.